Supporting Information: Rates of change in natural and anthropogenic radiative forcing over the past 20,000 years

Fortunat Joos and Renato Spahni

S1. Gas diffusion and enclosure model

Here we use a one dimensional gas diffusion and enclosure model (1) to calculate the width of the age distribution for the different trace gases and ice core sites. The width depends mainly on the accumulation rate and the annual mean temperature of the site and on the molecular diffusion coefficient of the trace gas. The distribution is smallest for sites with very high accumulation rates and temperatures, e.g. Law Dome at present conditions, and widest for sites with very low accumulation rates and temperatures, e.g. EPICA Dome C at glacial conditions. Since a major part of the greenhouse gas data is based on measurements on the EPICA Dome C ice core and the smoothing effect is strongest at this site, we calculated age distributions especially for this site. For the present (Last Glacial Maximum (LGM)) Antarctic climate conditions a Dome C site temperature of –54° C (–64° C) and an accumulation rate of 29 kg/m^2/yr (13 kg/m^2/yr) is used. As an illustration how narrow age distributions from Greenland and Antarctic high accumulation rate/temperature ice cores compared to Dome C are, we calculate the GRIP age distribution for Holocene conditions (–31° C , 220 kg/m^2/yr). Figure 7 shows CO_2 and CH_4 age distributions at Dome C and GRIP for different climatic conditions. The distribution is asymmetric with a long tail at Dome C. The width of the distribution, as referred to in the main text, is calculated at half height of the maximum of the distribution.

S2. Attenuation of the anthropogenic greenhouse gas increases in ice cores

Additionally to the age distribution, the model calculates for a given set of climatic input parameters and a prescribed atmospheric evolution its corresponding attenuated signal as it would be recorded in the ice core. The calculations have been accomplished by using the conditions at EPICA Dome C, the site with the lowest accumulation rate among the sites used for the reconstruction of the greenhouse gases based on polar ice cores over the last 20 ka (Figure 1). The attenuation at Dome C serves as an extreme: if an atmospheric signal is not smoothed out at Dome C, it will not be smoothed out in any other ice core used for this study. The attenuated CO_2, CH_4 and N_2O increases are calculated for present and LGM conditions at Dome C. The reference attenuation is the maximum value of the mean from the present and LGM runs for each gas (see section S1 for climate parameters). Deduced rate of change from this mean have maximum values of 0.26 ppm yr^{-1} for CO_2, 2.7 ppb yr^{-1} for CH_4, 0.13 ppb yr^{-1} for

N_2O and 6.1 10^{-3} W m^{-2} yr^{-1} for their combined radiative forcing. Input data and results of these calculations are shown in Figure 8.

Comparing these attenuated greenhouse gas increases with those observed in ice cores over the last glacial cycle, the anthropogenic increase is clearly unique. First, the data resolution is sufficient to exclude with very high confidence (9 out of 10 chance to be correct) a concentration peak similar to the anthropogenic rise for the past 50,000 years for CO_2 (2-4), for the past 80,000 years for CH_4 (2, 3, 5-13) and for the past 16,000 years for N_2O (2, 14). Second, when calculating the rate of concentration change on the attenuated increases, the current rate of change is indeed much larger than the reconstructed changes in the past for CO_2, CH_4, and the combined greenhouse gas forcing (see Refs. above).

S3. Radiative forcing

Table 1 summarizes the equations used to calculate radiative forcing from the concentration and emission data. A few forcing components that contribute to the anthropogenic radiative forcing are not explicitly included or neglected in our quantitative assessment as our information on their rate of change is poor and/or their contributions, as estimated by (15), are small. Radiative forcing from tropospheric ozone, estimated to be +0.35 W m^{-2} (5% to 95% confidence range: +0.25 to +0.65) in year 2005, by black and organic carbon (+0.18±0.2 W m^{-2}), forcing from stratospheric water vapour effects from methane (0.07±0.05 W m^{-2}) and changes in stratospheric ozone (-0.05±0.1 W m^{-2}) are not explicitly considered. We estimate based on input data used to drive the BernCC model (16) that these forcing contributed with around 7 10^{-3} W m^{-2} yr^{-1} to the average rate of change of the past 40 years. Radiative forcing from dust (-0.1±0.2 W m^{-2}) and nitrate aerosols (-0.1±0.1 W m^{-2}) as well as forcing from altered albedo (-0.1±0.2 W m^{-2}) in response to changes in land use and black carbon aerosols on snow may have offset about half of the former rate. In conclusion, we infer that all these forcings together contribute to the rate of change in radiative forcing with a few 10^{-3} W per m^2 and year.

S4. Data and splines

In this section data sources, sample spacing, uncertainties of ice and firn data, and the technical details of the spline fitting procedure are presented.

The concentration records of the past 22,000 and 2000 years used to calculate rates of change are compiled from the following sources. For the 22,000 year record, ice and firn data for CO_2 are from (2, 3, 17-20), for CH_4 from (2, 3, 5, 6, 21-23), and for N_2O from (2, 14, 24, 25). The Dome C CO_2 date are used on the Dome C time scale as by (19). The CH_4 data from GRIP and Dome C are on the GRIP SS09 time scale. For the past 2000 years, ice and firn data from the Law

Dome site are used (17, 18, 26). Atmospheric data are from the NOAA/ESRL Global Monitorin Division, representing weekly-mean global average concentrations (23, 27) (and also Pers. Comm. from J. Butler, 2004; T. Conway, 2004; E.J. Dlugokencky, 2004), and from Mauna Loa, Hawaii (28).

Sample spacing for the composite CO_2 record is typically 100 years or less during the Holocene and around 200 years during the last transition, with more frequent sampling during periods of fast variations. For the composite CH_4 record, sample spacing is about 100 years during periods with slow variations and about 50 years otherwise. Sample spacing for N_2O is around 100 years for the past 20 ka. Sampling intervals are shorter for the Law Dome record of the past 2 ka (Figure 5d). CO_2 and CH_4 samples are taken about every 20 years during the last millennium and about every 30 to 60 years during 0 to 1000 AD, while N_2O is sampled less frequently before 1500 AD. Sampling resolution is high and a few years only over the industrial period. Data spacing for the GRIP record (Figure 1d) is of the order of 100 years. More samples have been analyzed around periods of large CH_4 variations such as the transition to the Bølling, the end of the Younger Dryas and the 8.2 ka event, when data spacing is about 30 to 50 years.

Measurement precision for the ice core samples is typically less than 1 ppm for the CO_2 data from Dome C, South Pole and Kohnen Station and 1.2 ppm for the Law Dome data. For CH_4, precision (1σ) is 4.1 ppb for the Law Dome data and 10 ppb for the GRIP, Eurocore, Dome C and South Pole data. For N_2O, uncertainties (1σ) varies among cores and is 1.1 ppb for the South Pole firn data, 3.7 ppb for the GRIP data, and 6.5 ppb for the Law Dome data. We consider a 40-year period and assume Gaussian error propagation to estimate upper bounds for the uncertainties in the rate of change. This yields 0.04 ppm yr^{-1} for CO_2, 0.7 ppb yr^{-1} for CH_4, and 0.2 ppb yr^{-1} for N_2O. This is small compared to the typical rates of increase during the industrial period.

Spline fit: The spline fit of (29) acts like a digital low-pass filter. The cut-off period, $T_{0.5}$, the period at which the signal is dampened by 50%, is a function of a free parameter, λ, the data spacing, Δt, and the weight assigned to an individual data point (the weight is taken to be proportional to the inverse of the square of the uncertainty, δ, assigned to an individual data point i):

$$T_{0.5} = 2\pi \left(\lambda \cdot \Delta t \cdot \delta_i^2 \right)^{0.25} \qquad \text{Equation 1}$$

Periods shorter than the cut-off period are further suppressed. The cut-off period is selected using an appropriate value for λ. λ has been determined individually for periods with similar data spacing. Then, the cut-off period is approximately constant over the period as the cut-off period only weakly depends on the data spacing.

The Law Dome and atmospheric records of the past 2000 years were smoothed with a cut-off period of 40 years to recover multi-decadal variability. A period of 40 years roughly corresponds to the resolution of the Law Dome data. The Law Dome ice and firn data used for the last 2,000 years have a width of the age distribution of up to 20 years (air age spread is 10-12 years for DE08/-2 ice samples, 18-20 years for DSS ice samples and 5 years for DSSW20K firn air samples) (17). Uncertainties in dating is less than 3 years for the Law Dome DE08 and DE08 cores and less than $\pm$5 years for the DSS cores (17).

The cut-off frequencies for the 22,000-year records have been selected for different parts of the record by taking into account the data spacing and the width of the age distribution of the ice core measurements. The resulting spline fits follow the data very closely (Figure 1, 6). The technical details for the standard spline fits for the past 22,000 years are as follows. The records are divided into periods with relatively uniform data spacing. The CO_2 record was splined with a cut-off period of 500 years from 22 to 12 thousand years before present (ka BP) to follow also the relatively fast variations found during the transition. A cut-off period of 1000 years was used for the periods from 12 to 10 ka BP and from 10 to 2 ka BP. A cut-off period of 100 years is applied from 2 ka BP to 1850 AD and from 1850 AD to 1958 AD, and of 40 year from 1958 AD to 1978 AD (the period covered by Mauna Loa data) and from 1978 AD to 2005 AD when NOAA global air sampling data are available. The CH_4 data were fitted with a cut-off period of 300 years until 12 ka BP, with a cut-off period of 1000 years from 12 to 10 ka BP, with a cut-off period of 4000 years from 10 to 1 ka BP, with a cut-off period of 500 years from 1050 AD to 1750 AD, with a cut-off period of 300 years from 1750 AD to 1850 AD, with a cut-off period of 100 years from 1850 AD to 1980 AD, and with a cut-off period of 10 years from 1980 AD to 2004 AD. The N_2O record was splined with a cut-off period of 500 years for the periods from 16.4 to 11 ka BP, from 11 ka BP to 850 AD, and from 850 AD to 1600 AD, with a cut-off period of 200 years from 1600 AD to 1900 AD, with a cut-off period of 100 years from 1900 AD to 1977 AD, and of 40 years from 1977 AD to 2004 AD.

The Northern Hemisphere CH_4 data from GRIP and Eurocore and the NOAA data have been splined with a cut-off period of 600 years before 15 ka BP, with a cut-off period of 400 years from 14 to 12 ka BP and 11 to 8.6 ka BP and from 7.6 ka BP to 1400 AD, with a cut-off period of 100 years from 15 to 14 ka BP and 12 to 11 ka BP and 8.6 to 7.6 ka BP and from 1400 AD to 1980 AD, and with a cut-off period of 10 years from 1980 AD to 2005 AD.

The volcanic and solar forcing series of the last millennium and the record of halocarbons and SF_6 forcing were splined with a cut-off period of 40 years for comparison with forcing from CO_2, CH_4, and N_2O.

S5. Rates of change for selected periods

Average rates of change, r, for distinct periods are directly determined from the ice core data following:

$$r = \frac{c(t_2) - c(t_1)}{t_2 - t_1}, \qquad \text{Equation 2}$$

where c represents measured concentration, t_1, the time at the begin and t_2 at the end of the period. Tables 2 and 3 summarize the results for CO_2 and CH_4. The 20th century rate of change in CO_2 forcing is fourteen times larger and that for CH_4 forcing is more than four times larger than any sustained forcing changes computed for previous periods of the past 22,000 years.

S6. References

1. Spahni, R., Schwander, J., Flückiger, J., Stauffer, B., Chappellaz, J. & Raynaud, D. (2003) *Geophysical Research Letters* **30,** 1571, doi:10.1029/2003GL017093.
2. Flückiger, J., Monnin, E., Stauffer, B., Schwander, J., Stocker, T. F., Chappellaz, J., Raynaud, D. & Barnola, J. M. (2002) *Global Biogeochemical Cycles* **16,** 1010, doi:10.1029/2001GB001417.
3. Monnin, E., Indermühle, A., Dällenbach, A., Flückiger, J., Stauffer, B., Stocker, T. F., Raynaud, D. & Barnola, J. M. (2001) *Science* **291,** 112-114.
4. Indermühle, A., Stocker, T. F., Joos, F., Fischer, H., Smith, H. J., Wahlen, M., Deck, B., Mastroianni, D., Tschumi, J., Blunier, T., Meyer, R. & Stauffer, B. (1999) *Nature* **398,** 121-126.
5. Blunier, T., Chappellaz, J., Schwander, J., Stauffer, B. & Raynaud, D. (1995) *Nature* **374,** 46-49.
6. Chappellaz, J., Blunier, T., Kints, S., Dällenbach, A., Barnola, J. M., Schwander, J., Raynaud, D. & Stauffer, B. (1997) *Journal of Geophysical Research-Atmospheres* **102,** 15987-15997.
7. Chappellaz, J., Blunier, T., Raynaud, D., Barnola, J. M., Schwander, J. & Stauffer, B. (1993) *Nature* **366,** 443-445.
8. Dällenbach, A., Blunier, T., Flückiger, J., Stauffer, B., Chappellaz, J. & Raynaud, D. (2000) *Geophysical Research Letters* **27,** 1005-1008.
9. Flückiger, J., Blunier, T., Stauffer, B., Chappellaz, J., Spahni, R., Kawamura, K., Schwander, J., Stocker, T. F. & Dahl-Jensen, D. (2004) *Global Biogeochemical Cycles* **18,** GB1020, doi:10.1029/2003GB002122.
10. Huber, C., Leuenberger, M., Spahni, R., Flückiger, J., Schwander, J., Stocker, T. F., Johnsen, S. J., Landais, A. & Jouzel, J. (2006) *Earth and Planetary Science Letters* **243,** 504-519.
11. Spahni, R., Chappellaz, J., Stocker, T. F., Loulergue, L., Hausammann, G., Kawamura, K., Flückiger, J., Schwander, J., Raynaud, D., Masson-Delmotte, V. & Jouzel, J. (2005) *Science* **310,** 1317-1321.

12. Brook, E. J., Harder, S., Severinghaus, J., Steig, E. J. & Sucher, C. M. (2000) *Global Biogeochem. Cycles* **14,** 559-572.
13. Brook, E. J., Sowers, T. & Orchardo, J. (1996) *Science* **23,** 1087 - 1091.
14. Flückiger, J., Dällenbach, A., Blunier, T., Stauffer, B., Stocker, T. F., Raynaud, D. & Barnola, J. M. (1999) *Science* **285,** 227-230.
15. Forster, P., Ramaswamy, V., Artaxo, P., Berntsen, T., Betts, R., Fahey, D. W., Haywood, J., Lean, J., Lowe, D. C., Myhre, G., Nganga, J., Prinn, R., Raga, G., Schulz, M. & Van Doorland, R. (2007) in *Climate Change 2007: The Physical Science Basis. Contribution of Working Group I to Fourth Assessment Report of the Intergovernmental Panel on Climate Change*, eds. Solomon, S., Qin, D., Manning, M., Chen, Z., Marquis, M., Averyt, K. B., Tignor, M. & Miller, H. L. (Cambridge United Kingdom and New York, NY, USA, New York, NY, USA), pp. 129-234.
16. Joos, F., Prentice, I. C., Sitch, S., Meyer, R., Hooss, G., Plattner, G. K., Gerber, S. & Hasselmann, K. (2001) *Global Biogeochemical Cycles* **15,** 891-908.
17. Etheridge, D. M., Steele, L. P., Langenfelds, R. L., Francey, R. J., Barnola, J. M. & Morgan, V. I. (1996) *Journal of Geophysical Research-Atmospheres* **101,** 4115-4128.
18. MacFarling Meure, C. M., Etheridge, D., Trudinger, C., Steele, P., Langenfelds, R. L., van Ommen, T., Smith, A. & Elkins, J. W. (2006) *Geophysical Research Letters* **33,** L14810, doi:10.1029/2006GL026152.
19. Monnin, E., Steig, E. J., Siegenthaler, U., Kawamura, K., Schwander, J., Stauffer, B., Stocker, T. F., Morse, D. L., Barnola, J. M., Bellier, B., Raynaud, D. & Fischer, H. (2004) *Earth and Planetary Science Letters* **224,** 45-54.
20. Siegenthaler, U., Monnin, E., Kawamura, K., Spahni, R., Schwander, J., Stauffer, B., Stocker, T. F., Barnola, J. M. & Fischer, H. (2005) *Tellus Series B-Chemical and Physical Meteorology* **57,** 51-57.
21. Blunier, T., Chappellaz, J. A., Schwander, J., Barnola, J. M., Desperts, T., Stauffer, B. & Raynaud, D. (1993) *Geophysical Research Letters* **20,** 2219-2222.
22. Stauffer, B., Fischer, G., Neftel, A. & Oeschger, H. (1985) *Science* **229,** 1386-1388.
23. Steele, L. P., Dlugokencky, E. J., Lang, P. M., Tans, P. P., Martin, R. C. & Masarie, K. A. (1992) *Nature* **358,** 313-16.
24. Machida, T., Nakazawa, T., Fujii, Y., Aoki, S. & Watanabe, O. (1995) *Geophysical Research Letters* **22,** 2921-2924.
25. Battle, M., Bender, M., Sowers, T., Tans, P. P., Butler, J. H., Elkins, J. W., Ellis, J. T., Conway, T., Zhang, N., Lang, P. & Clarke, A. D. (1996) *Nature* **383,** 231-235.
26. Ferretti, D. F., Miller, J. B., White, J. W. C., Etheridge, D. M., Lassey, K. R., Lowe, D. C., MacFarling Meure, C. M., Dreier, M. F., Trudinger, C. M., van Ommen, T. D. & Langenfelds, R. L. (2005) *Science* **309,** 1714-1717.
27. Dlugokencky, E. J., Steele, L. P., Lang, P. M. & Masarie, K. A. (1994) *J. Geophys. Res.* **99,** 17021-17043.
28. Keeling, C. D. & Whorf, T. P. (2005) in *In Trends: A Compendium of Data on Global Change. Carbon Dioxide Information Analysis Center, Oak Ridge National Laboratory, U.S. Department of Energy, Oak Ridge, Tenn., U.S.A.*

29. Enting, I. G. (1987) *J. Geophys. Res.* **92,** 10977-10984.
30. Ramaswamy, V., Boucher, O., Haigh, J., Hauglustaine, D., Haywood, J., Myhre, G., Nakajima, T., Shi, G. Y. & Solomon, S. (2001) in *Climate Change 2001: The Scientific Basis. Contribution of Working Group I to the Third Assessment Report of the Intergovernmental Panel on Climate Change*, eds. Houghton, J. T., Ding, Y., Griggs, D. J., Noguer, M., van der Linden, P. J., Dai, X., Maskell, K. & Johnson, C. A. (Cambridge University Press, Cambridge, United Kingdom and New York, NY, USA, pp. 349-416.
31. Plattner, G.-K., Knutti, R., Joos, F., Stocker, T. F., von Bloh, W., Brovkin, V., Cameron, D., Driesschaert, E., Dutkiewicz, S., Eby, M., Edwards, N. R., Fichefet, T., Hargreaves, J. C., Jones, C. D., Loutre, M. F., Matthews, H. D., Mouchet, A., Mueller, S. A., Nawrath, S., Price, A., Sokolov, A., Strassmann, K. M. & Weaver, A. J. (2007) *Journal of Climate***,** in press.

277 **Table 1:** Equations to calculate radiative forcing relative to a preindustrial
278 reference concentration (C_0). The overlap in absorption bands between N_2O and
279 CH_4 is taken into account using the overlap function $f(M,N)=0.47\ \ln(1+2.01\times10^{-5}$
280 $(MN)^{0.75}+5.31\times10^{-15}\ M(MN)^{1.52})$. Direct and indirect sulfate aerosol forcing is
281 computed from anthropogenic, eSO_x, and natural, E_{nat}, sulfur emissions with
282 E_{nat}=42 TgS. Formulations for additional agents can be found in (16, 30) as
283 updated by (31)

agent	equation	C_o
CO_2	RF = 5.35 W m^{-2} $\ln(CO_2/CO_{2,o})$	278 ppm
CH_4	RF = 0.036 W m^{-2} $\left(\sqrt{CH_4}-\sqrt{CH_{4,0}}\right)$ $-\left(f\left(CH_4,N_2O_0\right)-f\left(CH_{4,0},N_2O_0\right)\right)$	742 ppb
N_2O	RF = 0.12 W m^{-2} $\left(\sqrt{N_2O}-\sqrt{N_2O_0}\right)$ $-\left(f\left(CH_{4,0},N_2O\right)-f\left(CH_{4,0},N_2O_0\right)\right)$	272 ppb
CFC-11	RF = 0.25 W m^{-2} ($CFC\text{-}11 - CFC\text{-}11_0$)	0 ppt
CFC-12	RF = 0.32 W m^{-2} ($CFC\text{-}12 - CFC\text{-}12_0$)	0 ppt
Tropospheric Sulphate	RF(S-direct) = -0.4 W m^{-2} $eSO_x(t)/\ eSO_x(t$=2000 AD)	
	RF(S-indirect)= -0.7 W m^{-2} $\ln((E_{nat}+eSO_x)/E_{nat})$ $(\ln((E_{nat}+eSO_x(\text{t=2000 AD})/E_{nat}))^{-1}$	

284

285 **Table 2:** Average rate of change in the CO_2 concentration (ppm = parts per
286 million by volume) and its radiative forcing for distinct periods of the past and for
287 the 20th century as evaluated using Equation 2 and the Dome C data. The
288 beginning and end of the periods for the Dome C records are given in thousand
289 years before 1950 AD (ka BP); numbers of digits are not representative for the
290 uncertainty of the age scale.

291

t_1 (ka BP)	t_2 (ka BP)	$c(t_1)$ (ppm)	$c(t_2)$ (ppm)	Δt (kyr)	Δc (ppm)	$\Delta c/\Delta t$ (ppm kyr^{-1})	$\Delta RF/\Delta t$ (W m^{-2} kyr^{-1})
- 20.797	- 17.292	184.4	188.5	3.505	4.2	1	34
- 17.292	- 15.682	188.5	219.4	1.610	30.9	19	504
- 15.682	- 14.565	219.4	228.5	1.117	9.1	8	195
- 14.565	- 14.270	228.5	239.1	0.294	10.6	36	825
- 14.270	- 12.748	239.1	237.5	1.522	-1.6	-1	-24
- 12.748	- 11.525	237.5	265.2	1.223	27.7	22	483
- 11.525	- 7.356	265.2	260.1	4.169	-5.1	-1	-25
- 7.356	- 0.434	260.1	282.0	6.922	21.8	3	62
1900 AD	2000 AD	296	367	0.100	71.	710	11,503

292

293 **Table 3:** As table 2, but for the GRIP CH_4 record (ppb = parts per billion by
294 volume) and age as thousand years before 1989 AD (ka BP). The overlapping
295 with N_2O has been neglected in the calculation of radiative forcing.
296

t_1 (ka BP)	t_2 (ka BP)	$c(t_1)$ (ppb)	$c(t_2)$ (ppb)	Δt (kyr)	Δc (ppb)	$\Delta c/\Delta t$ (ppb kyr^{-1})	$\Delta RF/\Delta t$ (W m^{-2} kyr^{-1})
- 20.803	- 16.685	365.0	364.0	4.118	-1.0	-0.2	-0.2
- 16.685	- 15.643	364.0	486.7	1.042	122.7	118	103
- 15.643	- 14.716	486.7	500.0	0.927	13.3	14	12
- 14.716	- 14.441	500.0	627.0	0.275	127.0	461	351
- 14.441	- 12.760	627.0	680.0	1.680	53.0	32	22
- 12.760	- 12.422	680.0	476.7	0.339	-203.3	-600	-451
- 12.422	- 11.715	476.7	475.0	0.706	-1.7	-2	-2
- 11.715	- 11.546	475.0	722.0	0.169	247.0	1,460	1,081
- 11.546	- 9.640	722.0	715.0	1.906	-7.0	-4	-2
- 9.640	- 5.195	715.0	573.0	4.445	-142.0	-32	-23
- 5.195	- 0.375	573.0	716.5	4.820	143.5	30	21
1900 AD	2000 AD	867	1755	0.100	888	8,880	4,481

297
298

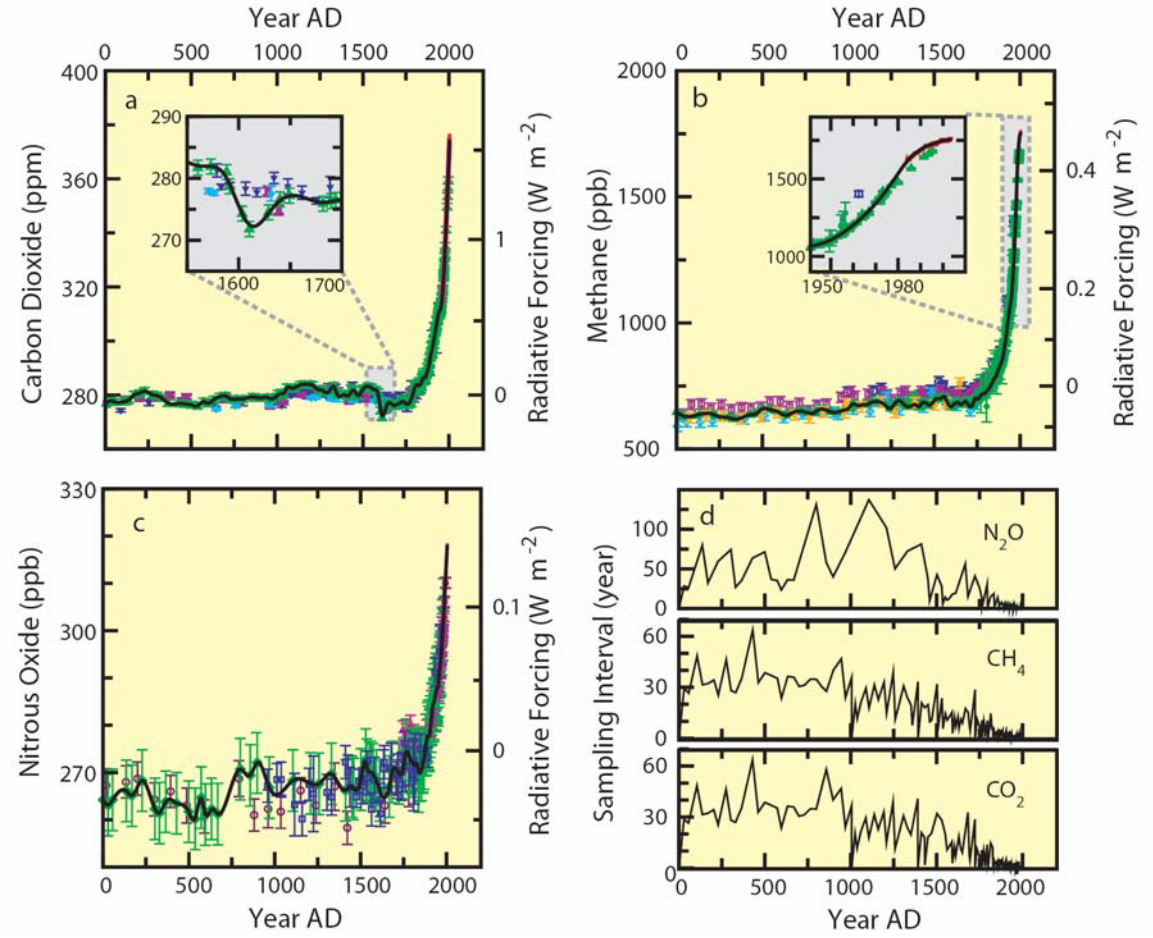

Figure 5: Evolution of (a) atmospheric CO_2, (b) methane, (c) and nitrous oxide over the past 2000 years. Radiative forcing relative to 1750 AD is shown on the right hand axis of panels a to c. Symbols denote ice and firn measurements and the red and magenta lines show measurements on atmospheric air samples from the NOAA/ESRL global network and from Mauna Loa, Hawaii. The black solid line is a spline fit with a cut-off period of 40 years through the high-resolution Law Dome ice and firn (green) (17, 18) and atmospheric samples as described in the main text. The recent decades of the CH_4 record were splined with a cut-off period of 10 years to capture the decrease in the CH_4 growth trend. The insets show details of the splines for selected periods. Panel d shows the sampling intervals for the Law Dome and atmospheric greenhouse gas data. Atmospheric data are from the NOAA/ESRL network (23, 27) (and also Pers. Comm. from J. Butler, 2004; T. Conway, 2004; E.J. Dlugokencky, 2004), and from Mauna Loa, Hawaii (28). Additional data, not used in the spline fit, are (a) for CO_2 from Dome C (magenta, square) (19), South Pole (diamond, blue) and Kohnen Station (triangle, dark) (20), (b) for CH_4 from the Eurocore (open circle,blue) (21) and GRIP (open square, magenta) ((5) and from D47 (diamond, cyan) (6), Siple (star, green) (22) and Dome C (star, orange) (2, 3), and (c) for N_2O from Dome C (circle) (2), H15 (triangle) (24), South Pole (star, violet) (25) and from GRIP and Eurocore (triangle, cyan) (14).

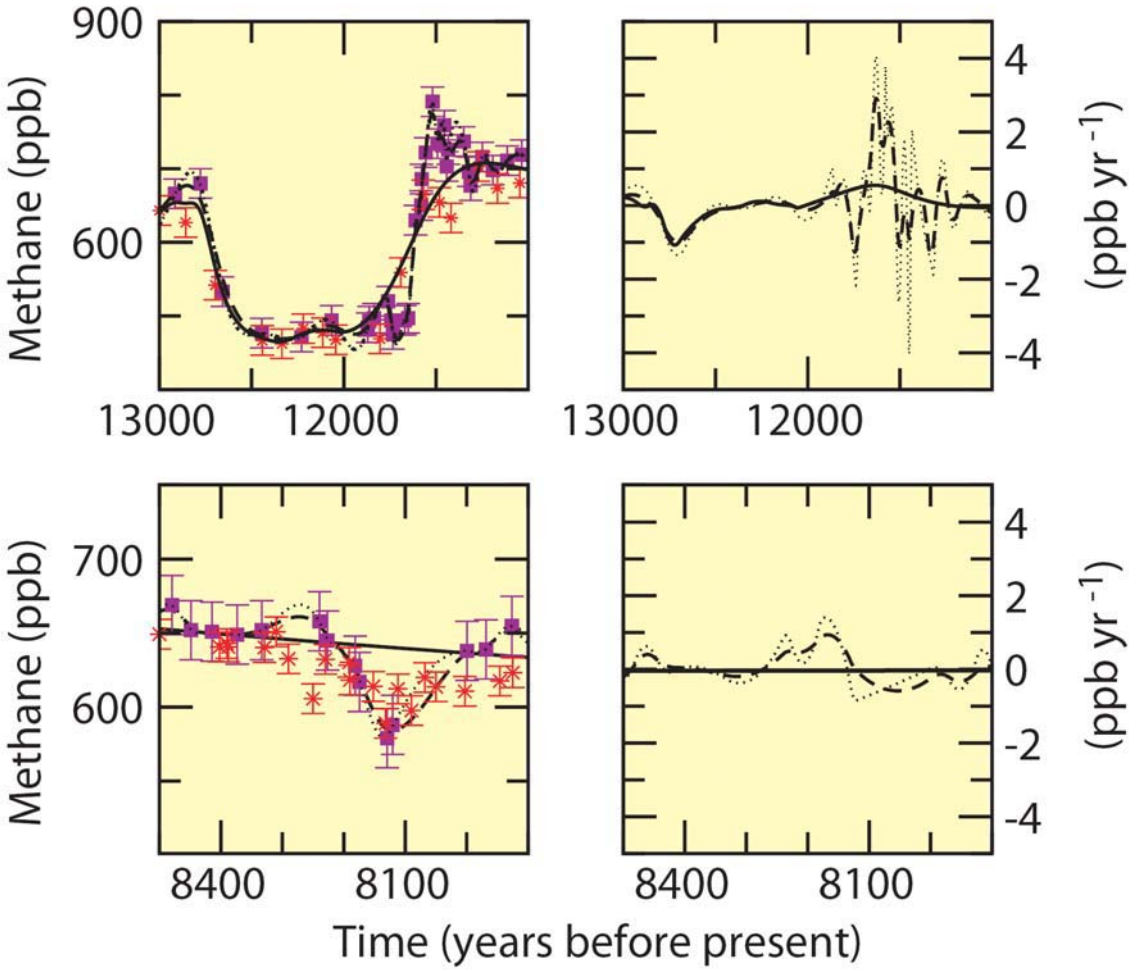

Figure 6: Details of the spline fits to the CH_4 record around the Younger Dryas and the 8.2 ka event. Left panels: CH_4 concentration from GRIP (square) and Dome C (star). The standard spline fit to the combined data is shown by the solid line, the standard fit to the Greenland data by the dashed line, and a high-frequency spline to the Greenland data by the dotted line. Right panels: Rates of change for CH_4 as calculated from the three splines. Here, the minima in the CH_4 concentration have been aligned by shifting the Dome C time scale by 90 years.

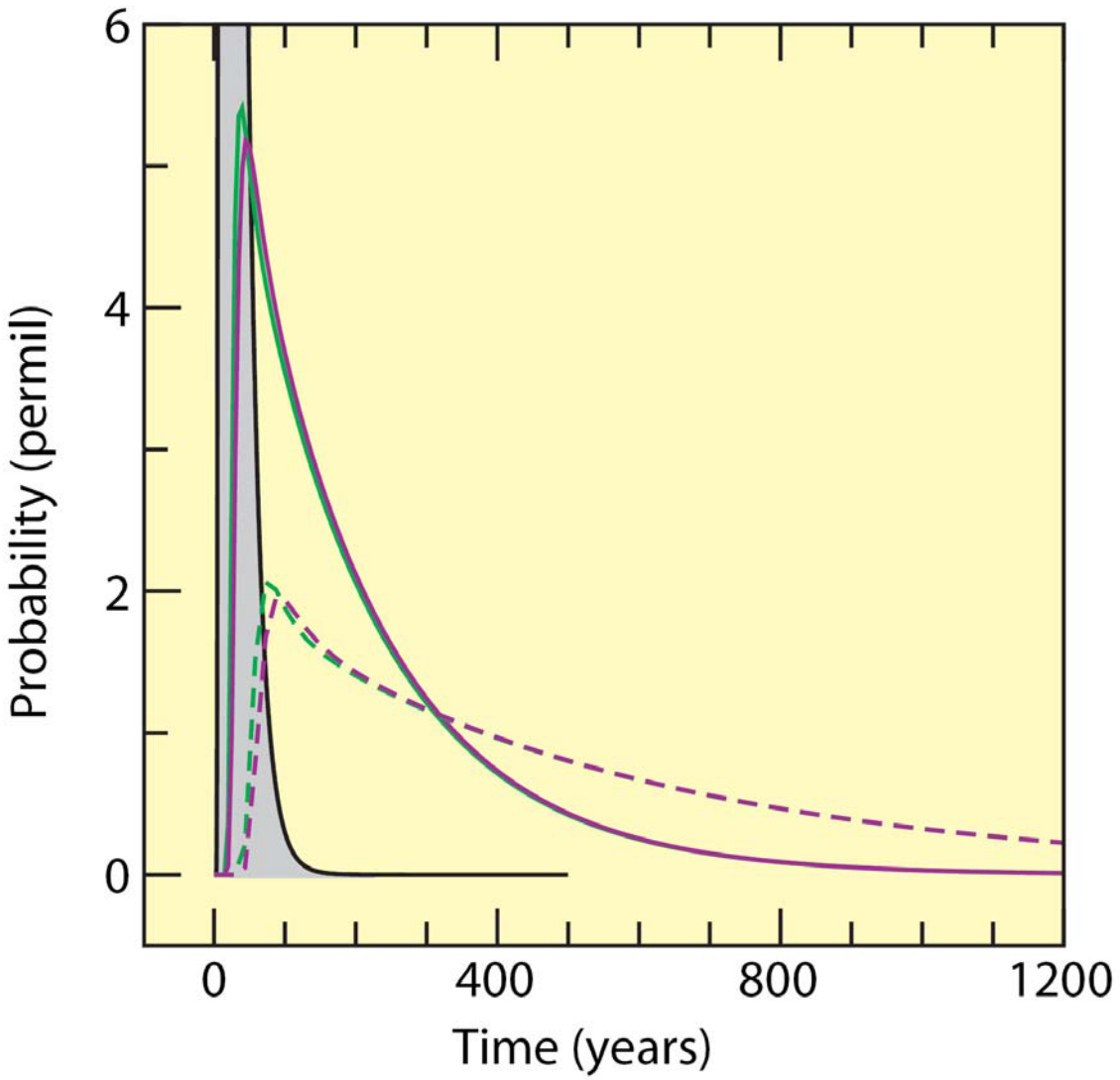

Figure 7: Age distribution of CO_2 and CH_4 in polar ice cores. The age distributions of CO_2 (violet) and CH_4 (green) in the bubbles of the EPICA Dome C core are calculated for current conditions (solid) and conditions during the Last Glacial Maximum (dash). The grey area represents the age distribution of CH_4 for the GRIP ice cores and the current interglacial. The Dome C age distributions of CO_2 and CH_4 differ only slightly for LGM conditions; the difference in the diffusion velocity is negligible compared to the very slow enclosure process, which is the same for both gases.

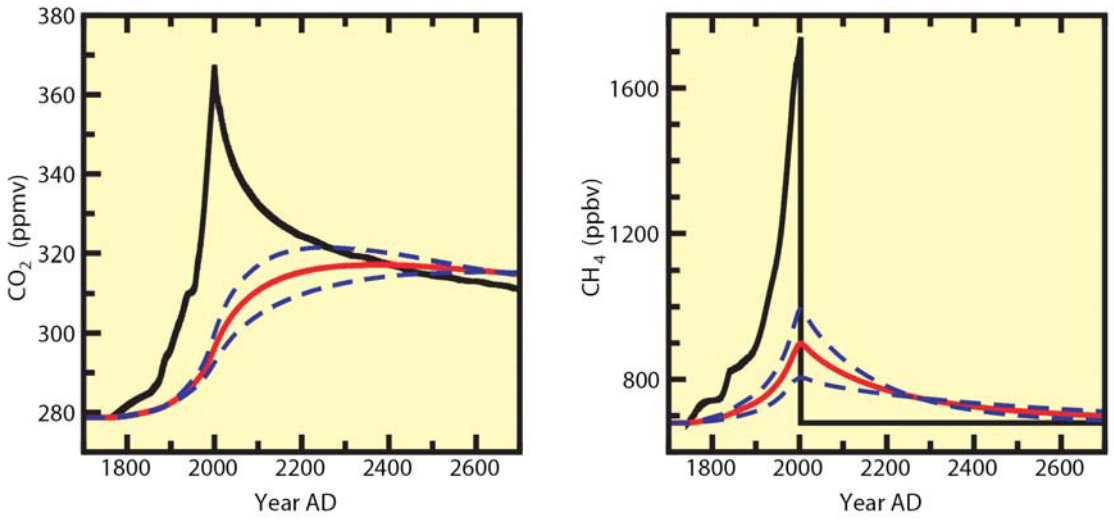

Figure 8: Attenuation of atmospheric greenhouse gas variations (black) during the enclosure process of air into firn and ice as modelled with a firn diffusion and enclosure model. The attenuated signals are calculated for present (upper blue) and Last Glacial Maximum conditions (lower blue). The reference attenuation used in the text is calculated as the maximum of the mean attenuated signal from both climate extremes (red). The atmospheric concentrations (black solid lines) of CO_2 (left) and CH_4 (right) are prescribed according to data until year 2000. Afterwards, anthropogenic emissions are assumed to cease completely and concentrations decrease. The atmospheric CO_2 decrease due to carbon uptake by the ocean and land biosphere is calculated with the Bern Carbon Cycle model. Atmospheric CH_4 is assumed to decrease instantaneously to the preindustrial concentration.